

**THE SYNTHESIS OF FUNCTIONALIZED-
SILICA/CARBON CATALYSTS FROM RICE
HUSK FOR THE CONVERSION OF HEXOSE
SUGAR INTO METHYL LEVULINATE AND
5-HYDROXYMETHYLFURFURAL**

**SYED MUHAMMAD AL-AMSYAR
BIN SYED ABD KADIR**

UNIVERSITI SAINS MALAYSIA

2018

**THE SYNTHESIS OF FUNCTIONALIZED-
SILICA/CARBON CATALYSTS FROM RICE
HUSK FOR THE CONVERSION OF HEXOSE
SUGAR INTO METHYL LEVULINATE AND
5-HYDROXYMETHYLFURFURAL**

by

**SYED MUHAMMAD AL-AMSYAR
BIN SYED ABD KADIR**

**Thesis submitted in fulfillment of the requirements
for the degree of
Doctor of Philosophy**

February 2018

ACKNOWLEDGEMENT

My greatest gratitude to my supervisor, Prof. Dr. Farook Adam, for his thoughtful advices, encouraging words, and continuous supervision. Deeply thanks to Dr. Anwar Iqbal, for his helpful guidance, comments, and helpful suggestions.

I would also like to express my appreciation to all professors and lecturers especially in School of Chemical Sciences for sharing their knowledge and expertise with me in order to complete this project. Not forgotten to all lab members. It has been such a pleasure to knowing you all.

I am truly thankful with the Skim Latihan Akademik IPTA (SLAI) awarded by Ministry of Higher Education and Universiti Malaysia Kelantan (UMK) for my PhD study. Also, a research grant from Universiti Sains Malaysia RUI grant 1001/PKIMIA/811269.

Last but not least, I would like to thank my parents, family members and beloved wife for their full support and encouragement during this project was executed.

TABLE OF CONTENTS

ACKNOWLEDGEMENT	ii
TABLE OF CONTENTS	iii
LIST OF TABLES	ix
LIST OF FIGURES	x
LIST OF APPENDICES	xvi
LIST OF ABBREVIATIONS	xvii
LIST OF SYMBOLS	xix
GRAPHICAL ABSTRACT	xx
ABSTRAK	xxi
ABSTRACT	xxiii
CHAPTER 1: INTRODUCTION AND LITERATURE REVIEW	1
1.1 Heterogeneous Catalysis.....	1
1.2 Heterogeneous Catalyst Precursor from Biological Waste	4
1.2.1 Waste from Shells.....	4
1.2.2 Waste from Rice Milling Industry	6
1.3 Utilization of Rice Husk	8
1.4 Silica/Carbon Composite in Heterogeneous Catalysis	10
1.5 Sugars as Chemical Feedstock	12

1.6	Mechanism of HMF Formation.....	18
1.6.1	HMF Formation from Dehydration of Hexoses by Heterogeneous Catalysts.....	22
1.6.1 (a)	Aqueous Solvent.....	22
1.6.1 (b)	Organic Solvents	26
1.7	Mechanism on Alkyl Levulinates Formation	33
1.8	Alkyl Levulinates Formation from Dehydration of Hexoses by Heterogeneous Catalysts.....	38
1.9	Formation of Humins.....	41
1.10	Problem Statement.....	47
1.11	Scope of Research	48
1.12	Objectives of Research	49
1.13	Thesis Outline.....	50
CHAPTER 2: EXPERIMENTAL AND METHODOLOGY		52
2.1	Chemicals	52
2.1.1	Pre-treatment of rice husk.....	52
2.1.2	The preparation of carbon from rice husk (C).....	53
2.1.3	The synthesis of silica (SiO ₂) from rice husk	53
2.1.4	The synthesis of silica/carbon (SiO ₂ /C) composites from rice husk	53
2.1.5	The synthesis of sulfonated-silica/carbon (SO ₃ H-SiO ₂ /C)	54

2.1.6	The synthesis of silica/carbon, silica, and carbon-supported aluminium oxide (Al-SiO ₂ /C-X, Al-SiO ₂ , and Al-C)	55
2.1.7	The synthesis of physically-mixed aluminium oxide (Al ₂ O ₃), silica (SiO ₂), and carbon (C) (Al-SiO ₂ /C*)	55
2.1.8	Catalytic testing	56
	2.1.8 (a) Influence of reaction conditions	57
	2.1.8 (b) Reusability of the catalyst	57
2.2	Characterizations	57
2.2.1	Scanning Electron Microscope (SEM)	57
2.2.2	Energy Dispersive X-Ray (EDX)/Elemental Mapping	58
2.2.3	X-Ray Diffraction (XRD)	59
2.2.4	X-ray Photoelectron Spectroscopy (XPS)	60
2.2.5	N ₂ Adsorption-Desorption	62
2.2.6	Attenuated Total Reflection (ATR) Fourier Transform Infra-Red (FTIR)	63
2.2.7	Pyridine-probe Fourier Transform Infra-Red (FTIR)	64
2.2.8	Thermogravimetric Analysis (TGA)	65
2.2.9	Ammonia-Temperature Programming Desorption (NH ₃ -TPD)	65
2.2.10	Nuclear Magnetic Resonance (NMR)	65
2.2.11	Pearson's Correlation Coefficient Test	66
2.2.12	Evaluation	67
CHAPTER 3: CHARACTERIZATION OF THE CATALYSTS.....		68

3.1	Modification with sulfonic acid group (SiO ₂ /C-SO ₃ H catalysts).....	68
3.1.1	SEM-EDX analysis.....	68
3.1.2	FTIR analysis.....	71
3.1.3	NH ₃ -TPD analysis.....	73
3.1.4	XRD analysis.....	74
3.1.5	N ₂ sorption analysis.....	75
3.1.6	Thermogravimetric (TGA) analysis.....	82
3.2	Modification with aluminium oxide (Al-SiO ₂ /C catalysts).....	87
3.2.1	SEM-EDX analysis.....	87
3.2.2	X-ray Diffraction (XRD) analysis and Elemental Mapping.....	90
3.2.3	XPS analysis.....	93
3.2.4	Pyridine-probe FTIR analysis.....	96
3.2.5	FTIR spectra analysis.....	98
3.2.6	TGA analysis.....	99
3.2.7	N ₂ sorption analysis.....	102
CHAPTER 4: CONVERSION OF HEXOSE SUGARS INTO FINE CHEMICALS.....		111
4.1	The conversion of fructose.....	111
4.1.1	Introduction.....	111
4.1.2	Catalytic reaction.....	113
	4.1.2 (a) The screening of the catalysts.....	113

4.1.2 (b)	Correlation between catalytic performance and physicochemical properties	114
4.1.3	Optimization studies	118
4.1.3 (a)	Effect of molarity of H ₂ SO ₄ during catalyst preparation	118
4.1.3 (b)	Effect of fructose concentration	119
4.1.3 (c)	Effect of temperature	120
4.1.3 (d)	Effect of catalyst dosage	121
4.1.4	Recycling experiment	122
4.1.5	Synthesis of HMF	125
4.2	The conversion of glucose	125
4.2.1	Introduction	125
4.2.2	Catalytic reaction	127
4.2.2 (a)	The screening of the catalysts	127
4.2.2 (b)	Correlation between catalytic performance and physicochemical properties	130
4.2.3	Optimisation of reaction parameters with Al-SiO ₂ /C catalyst	133
4.2.3 (a)	Effect of Al loading	133
4.2.3 (b)	Effect of glucose concentration	134
4.2.3 (c)	Effect of temperature	135
4.2.3 (d)	Effect of catalyst dosage	136
4.2.3 (e)	Effect of solvents	137

4.2.4	One-pot reaction	138
4.2.5	Recycling experiment	139
CHAPTER 5: CONCLUSIONS AND RECOMMENDATIONS		142
5.1	Conclusion	142
5.2	Recommendations for future studies	145
REFERENCES		147
APPENDICES		

LIST OF TABLES

		Page
Table 1.1	Chemical compositions from egg shell.	5
Table 1.2	The formation of HMF from hexose sugar in aqueous medium.	26
Table 1.3	The formation of HMF from hexose sugar in organic/biphasic systems.	32
Table 1.4	The formation of alkyl levulinate from hexose sugar in alcoholic solvents.	40
Table 1.5	Reported by-products in fructose decomposition in water (Antal, et al., 1990).	42
Table 1.6	Compositions of glucose and fructose-derived humins (Rasrendra, et al., 2013).	47
Table 2.1	The chemicals, their brands, and purity grades.	52
Table 3.1	The elemental analysis and sulfur-to-carbon weight ratio of various sulfonated silica/carbon catalysts by using EDX.	70
Table 3.2	The summary of textural data of sulfonated silica/carbon catalysts.	78
Table 3.3	SiO ₂ /C ratio of SO ₃ H-SiO ₂ /C-catalysts at different carbonization temperature.	101
Table 3.4	The summary of textural data of silica/carbon-supported aluminium oxide composites.	107
Table 4.1	Catalyst screening for synthesis of methyl levulinate.	113
Table 4.2	Pearson's correlation coefficient between physicochemical properties and TON.	117
Table 4.3	The comparison of textural data between fresh and reused catalyst.	124
Table 4.4	Synthesis of HMF by sulfonated silica/carbon catalysts.	125
Table 4.5	Pearson's correlation coefficient between physicochemical properties and the rate of HMF formation.	131
Table 4.6	The summary of textural data of Al-SiO ₂ /C-400 catalyst before and after recycling experiments.	141

LIST OF FIGURES

		Page
Figure 1.1	Chemical structure of (i) chitin and (ii) chitosan.	6
Figure 1.2	The anatomy of rice. Retrieved from http://www.bernas.com.my/index.php/rice-pedia/rice-anatomy .	7
Figure 1.3	Formation of silica on the cell wall of rice husk (Tabata, et al., 2010).	8
Figure 1.4	Fabrication of hierarchical porous carbon from rice husk (Tabata et al., 2010).	10
Figure 1.5	The biomass feedstock and their chemical structure (Alonso et al., 2010).	13
Figure 1.6	Lignocellulosic components in biomass (Alonso et al., 2010).	14
Figure 1.7	Feedstock from biomass and potential as chemical platform for biofuels.	16
Figure 1.8	Various chemical intermediates from HMF (Van Putten, et al., 2013).	17
Figure 1.9	Acyclic pathway of HMF formation from hexoses.	19
Figure 1.10	Plausible mechanism of fructose dehydration by DMSO as catalyst (Van Putten, et al., 2013).	20
Figure 1.11	Cyclic pathway of HMF formation from fructose (Van Putten, et al., 2013).	21
Figure 1.12	The Lewis acid site in niobic acid (Nakajima, et al., 2011).	25
Figure 1.13	The reaction pathway of anhydroglucose and HMF formation catalyzed by acid and base catalysts (Ohara, et al., 2010).	29
Figure 1.14	Illustration of biphasic system of sugar conversion (Román-Leshkov, et al., 2006).	30
Figure 1.15	Proposed reaction pathways of glucose-fructose-HMF by Sn-mont (Wang, et al., 2012).	31
Figure 1.16	Plausible reaction pathways of alkyl levulinate formation (Démolis, et al., 2014).	34
Figure 1.17	Reaction pathway of methyl levulinate formation via methyl glucoside intermediate (Peng et al., 2012).	35

Figure 1.18	Plausible formation of ethyl levulinate and ethyl glucopyranoside from sugars (Saravanamurugan, et al., 2011).	37
Figure 1.19	The plausible reaction between HMF and 2,5-dioxo-6-hydroxy-hexanal that contribute to humins growth (Patil & Lund, 2011).	43
Figure 1.20	Proposed structure of humins derived from glucose (Van Zandvoort, et al., 2013).	44
Figure 1.21	Revised model of glucose-derived humin structure based on the present NMR study (van Zandvoort, et al., 2015).	45
Figure 1.22	Plausible structure of glucose-derived humin after alkaline treatment (van Zandvoort et al., 2015).	46
Figure 2.1	Sulfonated silica/carbon catalyst at different carbonization temperature. From left to right; 250, 300, 350, 400, and 450 °C.	54
Figure 2.2	From left to right; Al-SiO ₂ /C-350, Al-SiO ₂ /C-400, Al-SiO ₂ /C-450, Al-C-400, Al-SiO ₂ , and Al-SiO ₂ /C*.	55
Figure 2.3	Ace pressure tube for catalytic reactions.	56
Figure 2.4	The basic principle of X-ray emission from an atom.	59
Figure 2.5	Visualization of Bragg's equation (Birkholz, 2006).	60
Figure 2.6	The principle of photoelectric effect. The binding energy could be calculated from this formula; $BE = hv(\text{known}) - KE(\text{calculated}) - \Phi(\text{calibrated})$.	61
Figure 2.7	Schematic diagram of N ₂ adsorption. Retrieved from http://www.micromeritics.com/Repository/Files/Gas_Adsorption_Theory_poster.pdf .	62
Figure 2.8	Multiple internal reflections in the ATR crystal contacted with the sample Retrieved from https://shop.perkinelmer.com/content/technicalinfo/tch_ftiratr.pdf .	64
Figure 3.1	The SEM images of sulfonated-silica/carbon catalysts at 20k magnifications. (a) SO ₃ H-SiO ₂ /C-250; (b) SO ₃ H-SiO ₂ /C-300; (c) SO ₃ H-SiO ₂ /C-350; (d) SO ₃ H-SiO ₂ /C-400; (e) SO ₃ H-SiO ₂ /C-450.	69
Figure 3.2	The graph of S/C wt. % ratio versus carbonization temperature of rice husk for the SO ₃ H-SiO ₂ /C catalyst.	71

Figure 3.3	The FTIR spectra for a) SO ₃ H-SiO ₂ /C-250; b) SO ₃ H-SiO ₂ /C-300; c) SO ₃ H-SiO ₂ /C-350; d) SO ₃ H-SiO ₂ /C-400; e) SO ₃ H-SiO ₂ /C-450; f) SO ₃ H-C-400. The functional groups are i) C=O carboxyl; ii) C=C aromatic; iii) O=S=O stretching; iv) Si-O-Si stretching; v) SO ₃ ⁻ stretching vi) Si-OH stretching; and vii) Si-O-Si bending.	72
Figure 3.4	The NH ₃ -TPD profiles for a) SO ₃ H-SiO ₂ /C-250; b) SO ₃ H-SiO ₂ /C-300; c) SO ₃ H-SiO ₂ /C-350; d) SO ₃ H-SiO ₂ /C-400; e) SO ₃ H-SiO ₂ /C-450.	74
Figure 3.5	The XRD for various sulfonated silica/carbon catalysts a) SO ₃ H-SiO ₂ /C-250; b) SO ₃ H-SiO ₂ /C-300; c) SO ₃ H-SiO ₂ /C-350; d) SO ₃ H-SiO ₂ /C-400; e) SO ₃ H-SiO ₂ /C-450.	75
Figure 3.6	The nitrogen sorption isotherm of a) SO ₃ H-SiO ₂ /C-250; b) SO ₃ H-SiO ₂ /C-300; c) SO ₃ H-SiO ₂ /C-350; d) SO ₃ H-SiO ₂ /C-400; e) SO ₃ H-SiO ₂ /C-450.	76
Figure 3.7	The pore distribution of a) SO ₃ H-SiO ₂ /C-250; b) SO ₃ H-SiO ₂ /C-300; c) SO ₃ H-SiO ₂ /C-350; d) SO ₃ H-SiO ₂ /C-400; e) SO ₃ H-SiO ₂ /C-450.	77
Figure 3.8	The graph of surface area of SO ₃ H-SiO ₂ /C catalyst versus carbonization temperature of rice husk.	79
Figure 3.9	The graph of total pore volume of SO ₃ H-SiO ₂ /C catalyst versus carbonization temperature of rice husk.	80
Figure 3.10	The graph of average pore width of SO ₃ H-SiO ₂ /C catalyst versus carbonization temperature of rice husk.	81
Figure 3.11	The thermograms of SO ₃ H-SiO ₂ /C-250.	82
Figure 3.12	The thermograms of SO ₃ H-SiO ₂ /C-300.	83
Figure 3.13	The thermograms of SO ₃ H-SiO ₂ /C-350.	84
Figure 3.14	The thermograms of SO ₃ H-SiO ₂ /C-400.	85
Figure 3.15	The thermograms of SO ₃ H-SiO ₂ /C-450.	86
Figure 3.16	SEM images of (a) SiO ₂ /C-400 and (b) Al-SiO ₂ /C-400 at 5k magnification.	88
Figure 3.17	SEM image of (a) nanosized Al-SiO ₂ /C-400 at 30k magnification and (b) further enlargement of its nanoparticles at 160k magnification	89

Figure 3.18	The EDX analysis of nanosized Al-SiO ₂ /C-400 catalyst particles.	90
Figure 3.19	The XRD pattern for SiO ₂ /C-400 composite (a) before and (b) after Al grafting.	91
Figure 3.20	(a) The SEM image of bulk Al-SiO ₂ /C-400 at a 100k magnification and its elemental mapping of its element. (b) the distribution of Al (c) the distribution of Si (d) the distribution of O and (e) the distribution of C atoms.	92
Figure 3.21	Wide scan of XPS spectrum of Al-SiO ₂ /C.	93
Figure 3.22	The XPS peak of Al 2p.	94
Figure 3.23	The XPS peak of Si 2p Al-SiO ₂ /C.	95
Figure 3.24	The XPS peak of C 1s of Al-SiO ₂ /C.	96
Figure 3.25	The pyridine adsorption study. (a) FTIR after pyridine sorption and evacuation of SiO ₂ /C and Al-SiO ₂ /C at 25 °C. Hydrogen-bound pyridine (H), Brønsted acid (B), Lewis acid (L), weak Lewis acid (WL).	97
Figure 3.26	FTIR spectra for Al-SiO ₂ /C-x at different carbonization temperature (i) x = 350 °C; (ii) x = 400 °C; (iii) x = 450 °C; and (iv) x = 500 °C.	98
Figure 3.27	TGA thermograms of Al-SiO ₂ /C-350.	99
Figure 3.28	TGA thermograms of Al-SiO ₂ /C-400.	100
Figure 3.29	TGA thermograms of Al-SiO ₂ /C-450.	101
Figure 3.30	The N ₂ sorption isotherm (a) before and (b) after Al grafting on SiO ₂ /C-400.	102
Figure 3.31	The pore size distribution (a) before and (b) after Al grafting on SiO ₂ /C-400.	103
Figure 3.32	The N ₂ sorption isotherm of Al-SiO ₂ /C-350.	104
Figure 3.33	The pore size distribution of Al-SiO ₂ /C-350.	104
Figure 3.34	The N ₂ sorption isotherm of Al-SiO ₂ /C-450.	105
Figure 3.35	The pore size distribution of Al-SiO ₂ /C-450.	106
Figure 3.36	The graph of average pore width of Al-SiO ₂ /C catalyst versus carbonization temperature of rice husk.	108

Figure 3.37	The graph of total pore volume of Al-SiO ₂ /C catalyst versus carbonization temperature of rice husk.	109
Figure 3.38	The graph of average pore width of Al-SiO ₂ /C catalyst versus carbonization temperature of rice husk.	109
Figure 4.1	Plausible pathway of levulinate esters formation from fructose.	112
Figure 4.2	The correlation between silica-to-carbon weight ratio with TON and fructose concentration reduction of each catalyst.	116
Figure 4.3	The effect of H ₂ SO ₄ concentration. Reaction conditions: SO ₃ H-SiO ₂ /C-350 50 mg, fructose 0.5 mmol, MeOH 3 mL, 7 h, 150 °C.	118
Figure 4.4	The effect of fructose concentration: Reaction condition: SO ₃ H-SiO ₂ /C-350 50 mg, MeOH 3 mL, 7 h, 150 °C.	119
Figure 4.5	The effect of temperature. Reaction conditions: SO ₃ H-SiO ₂ /C-350 50 mg, fructose 0.5 mmol, MeOH 3 mL, 7 h.	120
Figure 4.6	The effect of the mass of the catalyst. Reaction conditions: Fructose 0.5 mmol, MeOH 3 mL, 7 h, 150 °C.	121
Figure 4.7	Recycling experiment of sulfonated silica-carbon composite. Reaction conditions: SO ₃ H-SiO ₂ /C-350 100mg, fructose 0.5 mmol, MeOH 3 mL, 165 °C, 7h.	122
Figure 4.8	TGA analysis of SO ₃ H-SiO ₂ /C-350 catalyst before and after third recycling experiments.	123
Figure 4.9	The pore size distribution of reused SO ₃ H-SiO ₂ /C-350 catalyst.	124
Figure 4.10	The synthesis of HMF from glucose.	126
Figure 4.11	Catalyst screening for synthesis of HMF. Reaction conditions: Catalyst 100 mg, glucose 0.5mmol, NMP 4 mL, 170 °C, 5h. 0.04 mmol of Al content was used.	128
Figure 4.12	Elemental mapping of (a) Al, (b) Si, (c) C, and (d) O atoms from (e) a SEM image of a physical mixture of Al ₂ O ₃ , SiO ₂ , and C at 20k magnification.	129
Figure 4.13	The effect of varying carbon fraction on the rate of HMF production.	130
Figure 4.14	The catalytic dehydration of fructose into HMF by Al-SiO ₂ /C catalysts with different carbon contents.	132

Figure 4.15	The effect of Al loading onto silica/carbon composite on catalytic activity of glucose conversion into HMF. Reaction condition: catalyst 100 mg, glucose 1.0 mmol, NMP 4 mL, 170 °C, 5 h.	133
Figure 4.16	The effect of glucose concentration on catalytic activity of glucose conversion into HMF. Reaction condition: Al-SiO ₂ /C-400 catalyst 100 mg, NMP 4 mL, 170 °C, 5 h.	134
Figure 4.17	The effect of reaction temperature on catalytic activity of glucose conversion into HMF. Reaction condition: Al-SiO ₂ /C-400 catalyst 100 mg, glucose 1.0 mmol, NMP 4 mL, 5 h.	135
Figure 4.18	The effect of catalyst dosage on catalytic activity of glucose conversion into HMF. Reaction condition: Al-SiO ₂ /C-400 catalyst, glucose 1.0 mmol, NMP 4 mL, 170 °C, 5 h.	136
Figure 4.19	The effect of solvents on catalytic activity of glucose conversion into HMF. Reaction condition: Al-SiO ₂ /C-400 catalyst 100 mg, glucose 1.0 mmol, solvent 4 mL, 170 °C, 5 h.	137
Figure 4.20	Tandem glycosidic bond cleavage-isomerization-dehydration using Al-SiO ₂ /C-400 catalyst in one-pot reaction.	138
Figure 4.21	Recycling experiments of Al-SiO ₂ /C-400 in glucose conversion.	139
Figure 4.22	XRD pattern of Al-SiO ₂ /C-400 (a) before and (b) after fifth recycling experiments.	140
Figure 4.23	The N ₂ sorption isotherm of Al-SiO ₂ /C-400 after fifth recycling experiments.	140
Figure 4.24	The pore size distribution of Al-SiO ₂ /C-400 after fifth recycling experiments.	141

LIST OF APPENDICES

APPENDIX A

Figure A.1: EDX analysis data of SO ₃ H-SiO ₂ /C-250.	161
Figure A.2: EDX analysis data of SO ₃ H-SiO ₂ /C-300.	162
Figure A.3: EDX analysis data of SO ₃ H-SiO ₂ /C-350.	163
Figure A.4: EDX analysis data of SO ₃ H-SiO ₂ /C-400.	164
Figure A.5: EDX analysis data of SO ₃ H-SiO ₂ /C-450.	165

APPENDIX B

Figure B.1: EDX analysis data of Al-SiO ₂ /C-400.	166
Figure B.2: EDX analysis data of silica nanoparticle on Al-SiO ₂ /C-400.	167

APPENDIX C

Figure C.1: Quantification report of Al-SiO ₂ /C-400 catalyst from XPS analysis.	168
Figure C.2: XPS spectrum of Al 2p.	168
Figure C.3: XPS spectrum of C 1s.	169
Figure C.4: XPS spectrum of O 1s.	169
Figure C.5: XPS spectrum of Si 2p.	170

APPENDIX D

Figure D.1: Pattern search from ICDD of reused Al-SiO ₂ /C-400 catalyst.	171
---	-----

APPENDIX E

APPENDIX F

LIST OF ABBREVIATIONS

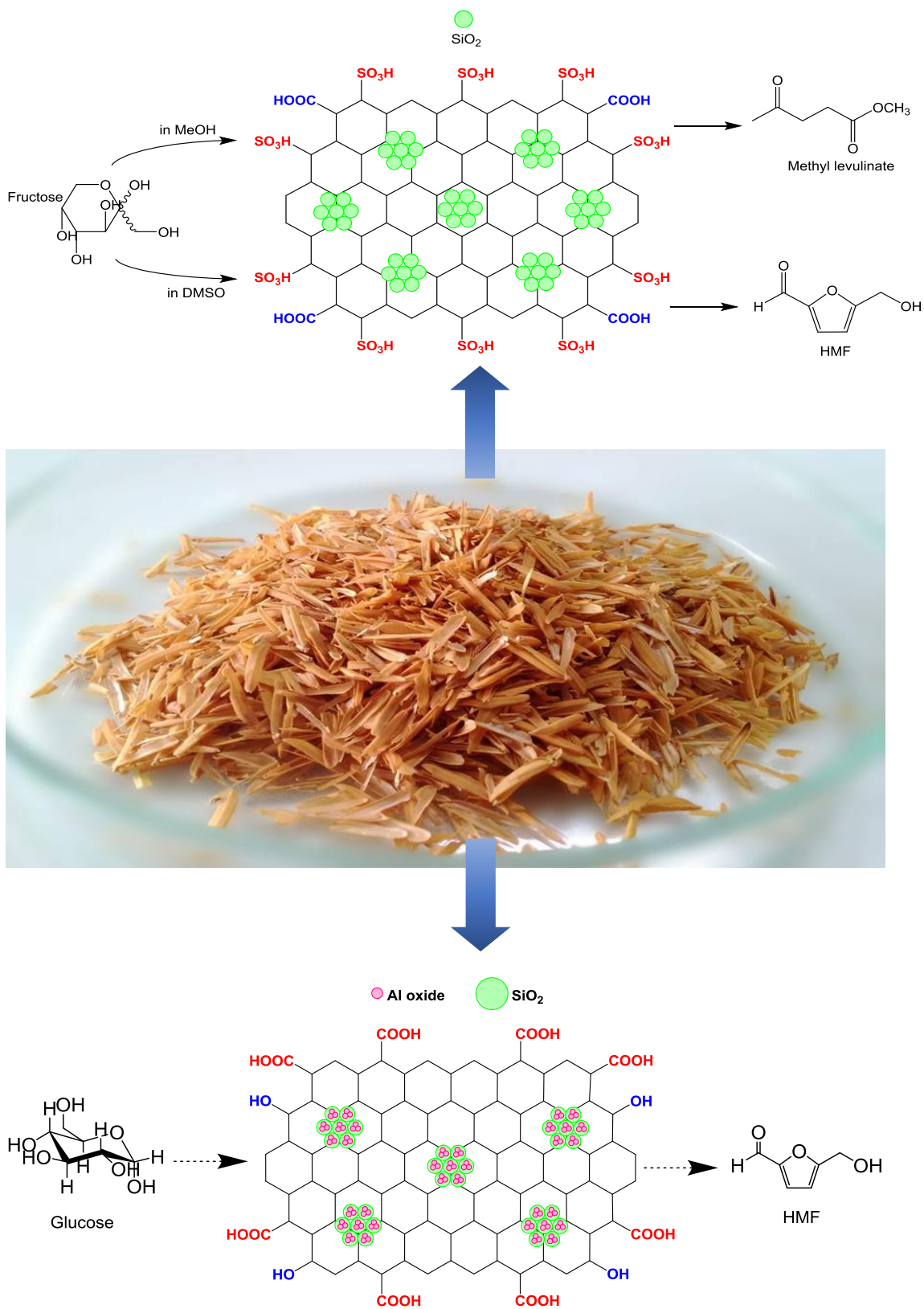
HMF	5-hydroxymethylfurfural
ML	Methyl levulinate
MML	5-methoxymethylfurfural
RH	Rice husk
RHA	Rice husk ash
MeOH	Methanol
FAME	Fatty acid methyl ester
MCM-41	Mobile Crystalline Materials-41
SBA-15	Santa Barbara Amorphous-15
LA	Levulinic acid
ALs	Alkyl levulinates
NMR	Nuclear magnetic resonance
DMSO	Dimethyl sulfoxide
VOP	Vanadyl phosphate
TON	Turn-over number
XRD	X-ray diffraction
NH ₃ -TPD	Ammonia-Temperature programming desorption

HPLC	High Performance Liquid Chromatography
GC	Gas chromatography
MS	Mass spectrometer
SEM	Scanning Electron Microscope
EDX	Energy Dispersive X-ray
XPS	X-ray Photoelectron Spectroscopy
ATR	Attenuated Total Reflection
FTIR	Fourier Transform Infra-Red
TGA	Thermogravimetric Analysis
DMF	Dimethylformamide
NMP	N-methylpyrrolidone
THF	Tetrahydrofuran
d-DMSO	Deuterated dimethyl sulfoxide
BET	Brunauer–Emmett–Teller
BJH	Barrett-Joyner-Halenda
S_{BET}	Surface area from BET method
V_{total}	Total pore volume
ICDD	International Centre for Diffraction Data

LIST OF SYMBOLS

-COOH	Carboxyl group
-SO ₃ H	Sulphonic group
-OH	Hydroxyl group
SiO ₂ + C-SO ₃ H	Physical mixture of silica and sulfonated carbon
RH*	Silica-removed rice husk
M	Molar
Å	Angstrom
2θ	Bragg angle
°C	Celsius degree

GRAPHICAL ABSTRACT



**SINTESIS PEMANGKIN SILIKA/KARBON YANG DIFUNGSIKAN
DARIPADA SEKAM PADI UNTUK PENUKARAN GULA HEKSOSA
KEPADA METIL LEVULINAT DAN 5-HIDROKSIMETILFURFURAL**

ABSTRAK

Mutakhir ini, komposit silika/karbon telah mendapat perhatian dalam pemangkinan heterogen disebabkan oleh sifat-sifat hibridnya yang unik. Namun, kesukaran dalam merekabentuk kaedah sintetik hijau tetap mencabar. Dalam kajian ini, pemangkin heterogen silika/karbon dengan komposisi yang pelbagai disediakan secara terus daripada sekam padi dengan memvariasikan suhu pengkarbonan (250, 300, 350, 400, dan 450 °C). Komposit yang disediakan ini telah difungsikan secara berasingan dengan asid sulfonik dan aluminium oksida lalu menghasilkan pemangkin-pemangkin berikut: silika/karbon tersulfonat ($\text{SO}_3\text{H-SiO}_2/\text{C-250}$, $\text{SO}_3\text{H-SiO}_2/\text{C-300}$, $\text{SO}_3\text{H-SiO}_2/\text{C-350}$, $\text{SO}_3\text{H-SiO}_2/\text{C-400}$, $\text{SO}_3\text{H-SiO}_2/\text{C-450}$) dan aluminium oksida yang disokong silika/karbon ($\text{Al-SiO}_2/\text{C-350}$, $\text{Al-SiO}_2/\text{C-400}$, dan $\text{Al-SiO}_2/\text{C-450}$). Untuk pemangkin $\text{SO}_3\text{H-SiO}_2/\text{C}$, data daripada XRD mengesahkan komposit ini adalah amorfus. Suhu pengkarbonan yang lebih tinggi menunjukkan peningkatan keliangan (saiz liang meningkat daripada 40 kepada 53 Å), jumlah isipadu liang (meningkat daripada 0.031 kepada 0.288 cm³/g), dan luas permukaan (meningkat daripada 39 kepada 260 m²/g). Analisis EDX menunjukkan nisbah berat silikon-kepada-karbon meningkat daripada 0.114 kepada 1.12 dengan peningkatan suhu pengkarbonan. Walaubagaimanapun, nisbah berat sulfur-kepada-karbon menurun

daripada 0.040 kepada 0.0055. Untuk pemangkin Al-SiO₂/C, data XPS membuktikan kehadiran aluminium di dalam bentuk Al₂O₃ (1.03 wt%). Data XRD mengesahkan pemangkin ini adalah amorfus. Analisis jerapan-nyahjerapan nitrogen menunjukkan tiada impak besar terhadap sifat tekstural selepas cantuman Al₂O₃, dengan luas permukaan hanya menurun daripada 179 kepada 141 m²/g. Jumlah isipadu liang mengecil daripada 0.155 kepada 0.124 cm³/g, dan lebar liang meningkat daripada 44 kepada 48 Å. Pemangkin SO₃H-SiO₂/C digunakan sebagai pemangkin asid Brønsted heterogen untuk penukaran fruktosa kepada metil levulinat (ML) dan 5-hidroksimetilfurfural (HMF). Hasil ML sebanyak 90% dapat diperoleh pada suhu 165 °C selama 7 jam dengan menggunakan pelarut metanol. Hasil ML menurun di dalam eksperimen pengitaran semula didorong oleh pengendapan karbon berterusan, yang akhirnya menyebabkan penyahaktifan mangkin. Komposit ini juga mampu menukarkan fruktosa kepada 56 – 74% hasil HMF di dalam pelarut dimetil sulfoksida (DMSO) pada suhu 130 °C selama 5 jam. Untuk pemangkin Al-SiO₂/C, ianya digunakan sebagai mangkin asid heterogen Lewis-Brønsted dwifungsian untuk menukarkan glukosa kepada HMF. Penggunaan pemangkin ini menghasilkan 52% HMF pada suhu 170 °C selama 5 jam dengan menggunakan pelarut N-metilpirrolidon (NMP). Pemangkin ini dibuktikan stabil tanpa penurunan hasil yang ketara selepas beberapa eksperimen pengitaran semula.

**THE SYNTHESIS OF FUNCTIONALIZED-SILICA/CARBON CATALYSTS
FROM RICE HUSK FOR THE CONVERSION OF HEXOSE SUGAR INTO
METHYL LEVULINATE AND 5-HYDROXYMETHYLFURFURAL**

ABSTRACT

Recently, silica/carbon composite material has received much attention in heterogeneous catalysis due to its unique hybrid properties. However, the difficulties in designing green synthetic methods remain challenging. In this study, varied proportion of silica/carbon heterogeneous catalyst was prepared directly from rice husk by varying the carbonization temperatures (250, 300, 350, 400, and 450 °C). The prepared composites were functionalized separately with sulfonic acid and aluminium oxide giving the following catalysts: sulfonated-silica/carbon (SO₃H-SiO₂/C-250, SO₃H-SiO₂/C-300, SO₃H-SiO₂/C-350, SO₃H-SiO₂/C-400, SO₃H-SiO₂/C-450) and silica/carbon-supported aluminium oxide (Al-SiO₂/C-350, Al-SiO₂/C-400, and Al-SiO₂/C-450). For the SO₃H-SiO₂/C catalysts, the XRD data confirms these composites were amorphous. Higher carbonization temperature showed an increase in porosity (pore size increased from 40 to 53 Å), total pore volume (increased from 0.031 to 0.288 cm³/g), and surface area (increased from 39 to 260 m²/g) of the composites. EDX analysis showed the silicon-to-carbon weight ratios of the composite increased from 0.114 to 1.12 with increase in carbonization temperature. However, the sulfur-to-carbon weight ratio showed a decrease from 0.040 to 0.0055. In the case of Al-SiO₂/C catalyst, XPS data showed the presence of aluminium in the form of Al₂O₃ (1.03 wt%).

The XRD data confirms this catalyst was amorphous. N₂ adsorption-desorption analysis shows no major impact on textural properties after Al₂O₃ grafting, as the surface area just decreased from 179 to 141 m²/g. The total pore volume decreased from 0.155 to 0.124 cm³/g, and the pore width increased from 44 to 48 Å. The SO₃H-SiO₂/C catalysts were used as heterogeneous Brønsted acid catalyst in the conversion of fructose into methyl levulinate (ML) and 5-hydroxymethylfurfural (HMF). A product yield of 90% of ML was obtained at 165 °C in 7 hours in methanol solvent. The yield decreased in the recycling experiments due to continued carbonaceous deposition resulting in deactivation. These composites were also able to convert fructose to HMF in 56 – 74% yield in dimethyl sulfoxide (DMSO) solvent at 130 °C in 5 hours. For the Al-SiO₂/C composite, it was used as a bifunctional heterogeneous Lewis-Brønsted acid catalyst to convert glucose into HMF. The use of the catalyst resulted in 52% yield of HMF at 170 °C in 5 hours in *N*-methylpyrrolidone (NMP) solvent. This catalyst was stable without significant loss of yield after several recycling experiments.

CHAPTER 1

INTRODUCTION AND LITERATURE REVIEW

1.1 Heterogeneous Catalysis

Heterogeneous catalyst is the form of catalysis where catalyst and reactant are in different physical phases. In most cases, the catalysts are solid and the reactants are in liquid or gaseous form (Rothenberg, 2008). Homogeneous catalysts are when the catalyst and reactant are in the same physical phase. Homogeneous catalysis offers high activity and selectivity due to the high degree of interaction. The limitation of pore diffusion is eliminated in homogeneous catalysis. However, the difficulty in separation and recovery of the catalysts are the main drawback of the homogeneous catalysts.

The development of heterogeneous catalyst is desirable because it possesses important properties, especially recyclability, facile preparation and separation. In addition, it can be separated by using simple filtration. These advantages meet the requirement for green chemical principles and processes (Anastas & Warner, 1998) The Twelve Principles of Green Chemistry are:

a) **Prevention**

It is better to prevent waste than to treat or clean up waste after it has been created.

b) Atom Economy

Synthetic methods should be designed to maximize the incorporation of all materials used in the process into the final product.

c) Less Hazardous Chemical Syntheses

Wherever practicable, synthetic methods should be designed to use and generate substances that possess little or no toxicity to human health and the environment.

d) Designing Safer Chemicals

Chemical products should be designed to affect their desired function while minimizing their toxicity.

e) Safer Solvents and Auxiliaries

The use of auxiliary substances (e.g. solvents, separation agents, etc.) should be made unnecessary wherever possible and innocuous when used.

f) Design for Energy Efficiency

Energy requirements of chemical processes should be recognized for their environmental and economic impacts and should be minimized. If possible, synthetic methods should be conducted at ambient temperature and pressure.

g) Use of Renewable Feedstocks

A raw material or feedstock should be renewable rather than depleting whenever technically and economically practicable.

h) **Reduce Derivatives**

Unnecessary derivatization (use of blocking groups, protection/deprotection, temporary modification of physical/chemical processes) should be minimized or avoided if possible, because such steps require additional reagents and can generate waste.

i) **Catalysis**

Catalytic reagents (as selective as possible) are superior to stoichiometric reagents.

j) **Design for Degradation**

Chemical products should be designed so that at the end of their function they break down into innocuous degradation products and do not persist in the environment.

k) **Real-time analysis for Pollution Prevention**

Analytical methodologies need to be further developed to allow for real-time, in-process monitoring and control prior to the formation of hazardous substances.

l) **Inherently Safer Chemistry for Accident Prevention**

Substances and the form of a substance used in a chemical process should be chosen to minimize the potential for chemical accidents, including releases, explosions, and fires.

In this work, the author will utilize renewable feedstock (e.g. sugars) as a substrate to produce fine chemicals (e.g. hydroxymethylfurfural and alkyl levulinate) by using heterogeneous catalyst from agricultural waste as a catalyst precursor. The

current trend in research is mainly directed towards the development of high-performance heterogeneous catalysts for environmental-friendly chemical processes (Kaneda, et al., 2006). Therefore, this work will at least fulfill two out of twelve Principles of Green Chemistry (g and i).

1.2 Heterogeneous Catalyst Precursor from Biological Waste

Large-scale productions of biological waste especially in Malaysia, despite causing disposal problems, provide various opportunities in catalysis. For instance, waste materials can be used as active materials and precursor for catalyst synthesis (Balakrishnan, et al., 2011). In general, there are two major sources of waste in Malaysia; shells and rice husk.

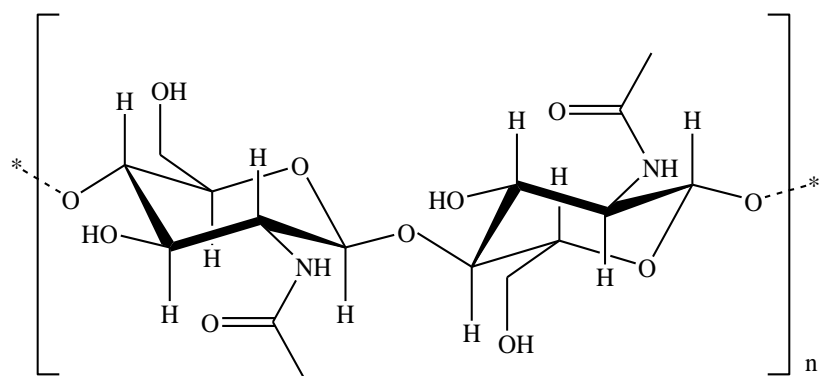
1.2.1 Waste from Shells

Shells mainly consists of CaCO_3 (Wei, et al., 2009). After thermal decomposition, CaO will be formed and release CO_2 gas. According to Tsai et al., (2008), despite consists of CaCO_3 , it also has trace amounts of MgCO_3 , $\text{Ca}_3(\text{PO}_4)_2$, and organic matters, as listed in Table 1.1. CaO has been used as a base catalyst in many catalytic reactions especially in transesterification to produce biodiesel. It has been reported that after calcination of powdered oyster shell above $700\text{ }^\circ\text{C}$, CaO act as a catalyst in esterification of soybean oil with more than 70% yield of high purity biodiesel (Nakatani, et al., 2009). Fly ash-supported CaO derived from egg shell has been used in transesterification of soybean oil to yield fuel grade biodiesel with higher fatty acid methyl ester (FAME) content (Chakraborty, et al., 2010).

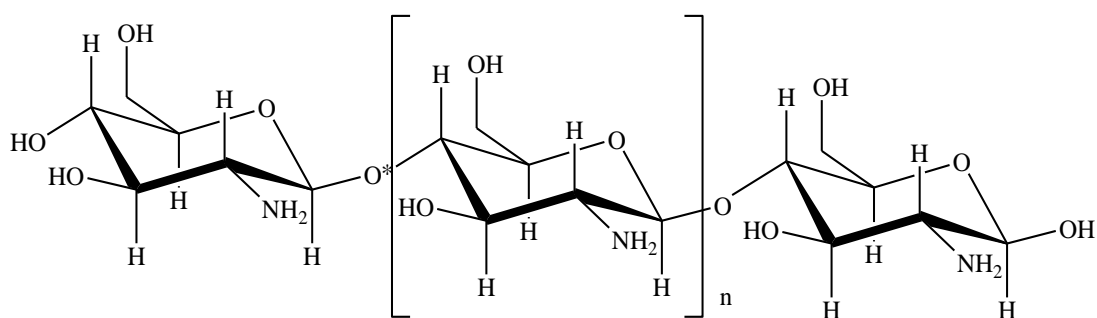
Table 1.1: Chemical compositions from egg shell.

Chemical compound	Weight percent (wt. %)
CaCO ₃	94
MgCO ₃	1
Ca ₃ (PO ₄) ₂	1
Organic matters	4

Waste mud crab (*Scylla serrata*) shell as CaO source have been employed to esterify palm oil (Boey, et al., 2009). Crab shells consist of chitin, second abundant biopolymer after cellulose, as shown in Figure 1.1(i). It is a long-chain polymer of an *N*-acetylglucosamine, one of the glucose derivatives. The annual production rate of chitin is enormous, and the number of literature regarding its application as catalyst support has been published is ever increasing (Macquarrie & Hardy, 2005). For instance, potassium fluoride (KF) loaded with incomplete carbonized shrimp shells has been demonstrated to become active catalyst in biodiesel production from rapeseed oil (Yang, et al., 2009). A conversion of 89.1% can be obtained after 3 hours reaction was carried out at 65 °C, 2.5 wt% catalyst, and 9:1 molar ratio of methanol/rapeseed oil. The authors claimed that the active site originated from the reaction of KF and incomplete carbonized shell. Figure 1.1(ii) illustrates the NH₂ groups in chitosan which could act as basic site for the base-catalyzed reactions.



(i)



(ii)

Figure 1.1: Chemical structure of (i) chitin and (ii) chitosan.

Thus, the utilization of shells as inorganic and organic components can be exploited, depending on the needs of the catalytic reaction. Shells from poultry industries can be used as a source of inorganic CaO for base-catalyzed reactions while crustacean's shells can be used as carbon-based materials for catalyst support.

1.2.2 Waste from Rice Milling Industry

In Malaysia, rice is the staple food. The paddy fields occupy vast area of land especially in the northern region (Kedah and Pulau Pinang). Therefore, the production of hefty amounts of rice husk is inevitable. Rice hull or rice husk (RH) which is produced from rice milling industry in Malaysia has been considered as one of the most abundant agricultural waste materials. Rice husk is the thin layer of material that

wraps the rice grain, protecting the grain as it grows and matures, as illustrated in Figure 1.2. The improper disposal of rice husk will create problems towards the environment.

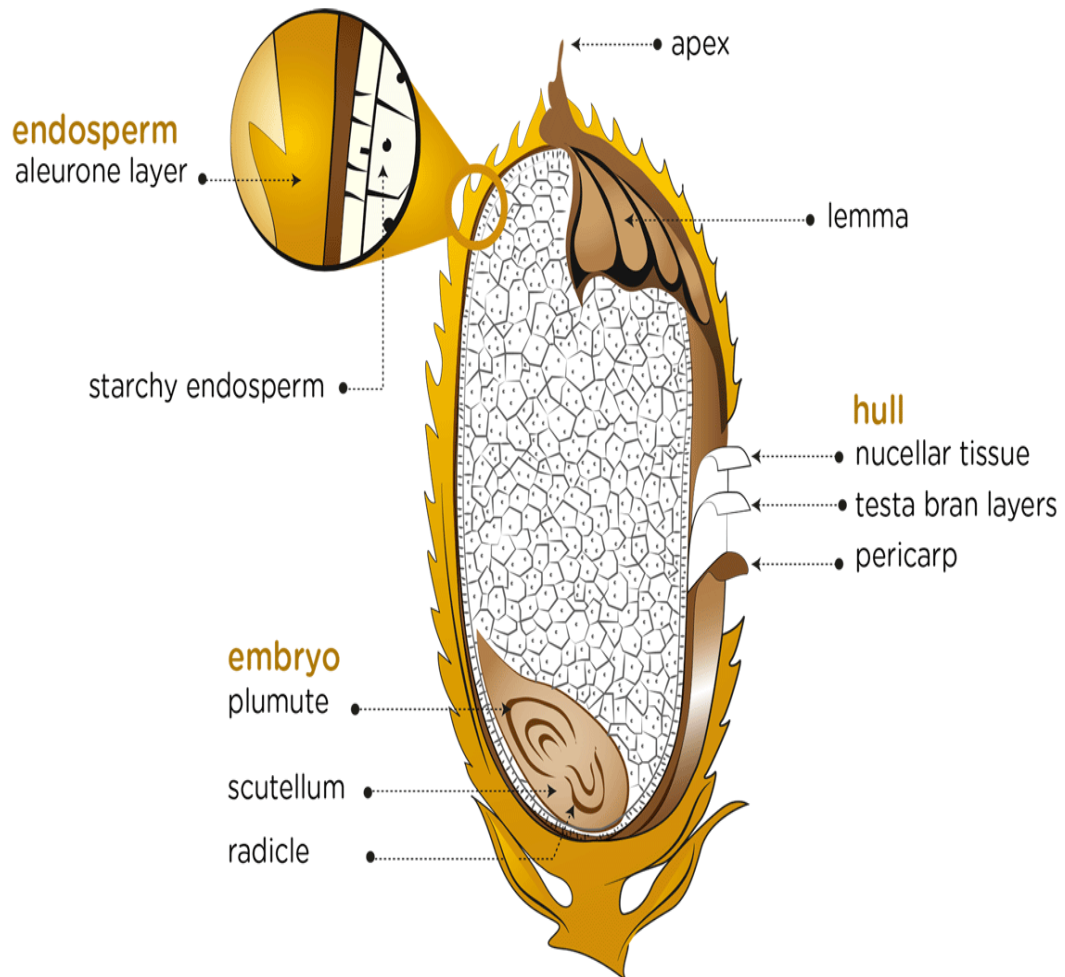


Figure 1.2: The anatomy of rice. Retrieved from <http://www.bernas.com.my/index.php/rice-pedia/rice-anatomy>.

Basically, silicic acid and water are taken into the plant via the roots from the soil (Ma & Takahashi, 2002). Amorphous silica can be found on the rice's cell wall on the surface of leaves, stems and husks in form of silica-cuticle and silica-cellulose double layers (Currie & Perry, 2007; Ma, et al., 2006). In addition, small and large silica particles also exist in the intercellular layers, as shown in Figure 1.3.

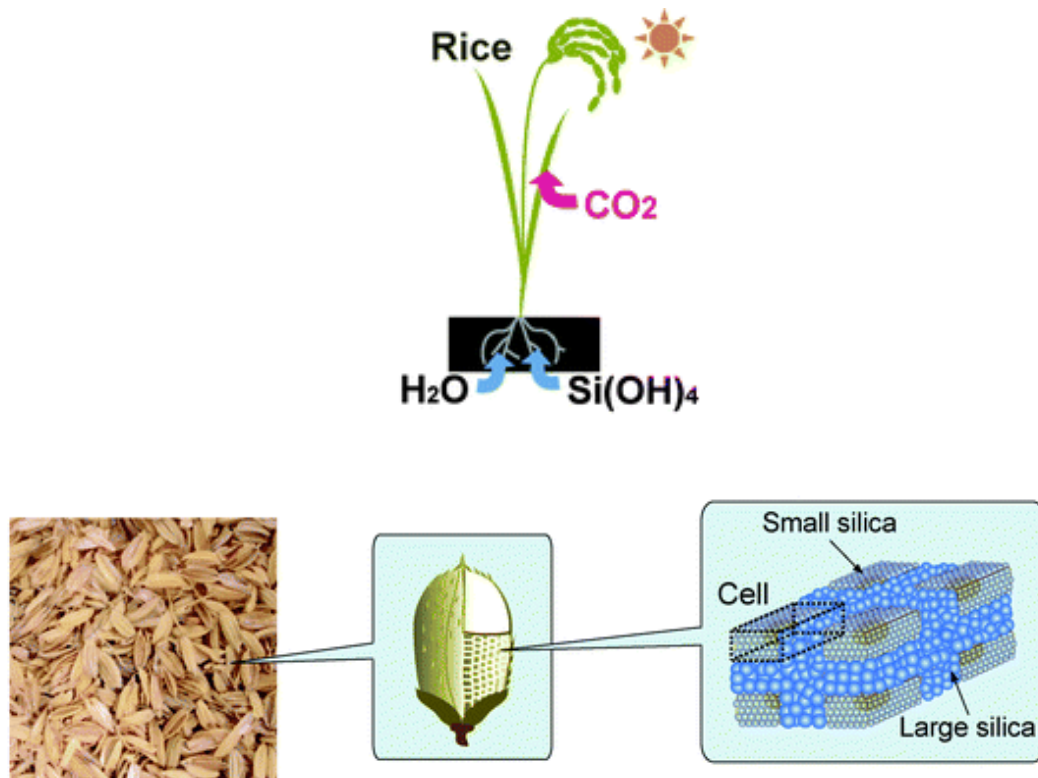


Figure 1.3: Formation of silica on the cell wall of rice husk (Tabata, et al., 2010).

1.3 Utilization of Rice Husk

Rice husk consist of 15 – 20% of silica (SiO_2) and its ash (RHA) contains about 95% SiO_2 depending on the temperature at which the RH is burnt. The RH also consists of cellulose, lignin, pentose, and other organic components. There are two common methods to obtain SiO_2 from rice husk; by calcination and solvent extraction. The latter is more environment-friendly (since open burning can cause health problems) and better purity of SiO_2 can be yielded. Under solvent extraction, the result of mixing rice husk in NaOH solution will produce silica in the form of sodium silicate and organic residues. By adding suitable amount of mineral acids into this solution, sodium silicate is converted into silica form.

Many examples of utilizing silica from rice husk as a catalyst precursor have been demonstrated. This catalyst framework has been demonstrated recently via grafting and sol-gel techniques. Furthermore, addition of surfactant will create pores in the solid structure. Such treatment can increase the surface area of the prepared catalyst. These catalysts showed good potential as heterogeneous catalysts such as in alkylation, benzylation, degradation of phenol, oxidation, and esterification (Adam, et al., 2012).

On the other hand, silica-removed rice husk (denoted as RH*) was produced too, mainly consists of cellulose, hemicelluloses, pentose, and lignin (James & Rao, 1986). This lignocellulosic biomass can be used as a substrate in conversion of sugars into fine useful chemical reagents (Alonso, et al., 2010). However, the fractionation is a difficult process and requires physical or chemical pretreatment for easier degradation of cellulose. Another alternative is to employ starch or shorter carbohydrates such as disaccharide or monosaccharide since complexity to isolate of sugars from lignocellulosic biomass could double the production cost.

Also, lignocellulosic components in rice husk can be transformed into carbon material by carbonization under air or N₂ atmosphere. Recently, silica in rice husk has been used as a natural template to synthesize hierarchical porous carbon, as depicted in Figure 1.4 (Tabata, et al., 2010). Whilst many researchers focusing on utilizing rice husk as a silica or carbon sources, the development of silica/carbon composite directly from rice husk are less reported. This composite have been widely used in transparent conductors (Watcharotone, et al., 2007), solar absorber (Mastai, et al., 2002), heterogeneous catalyst support (Wan, et al., 2009), and many more.

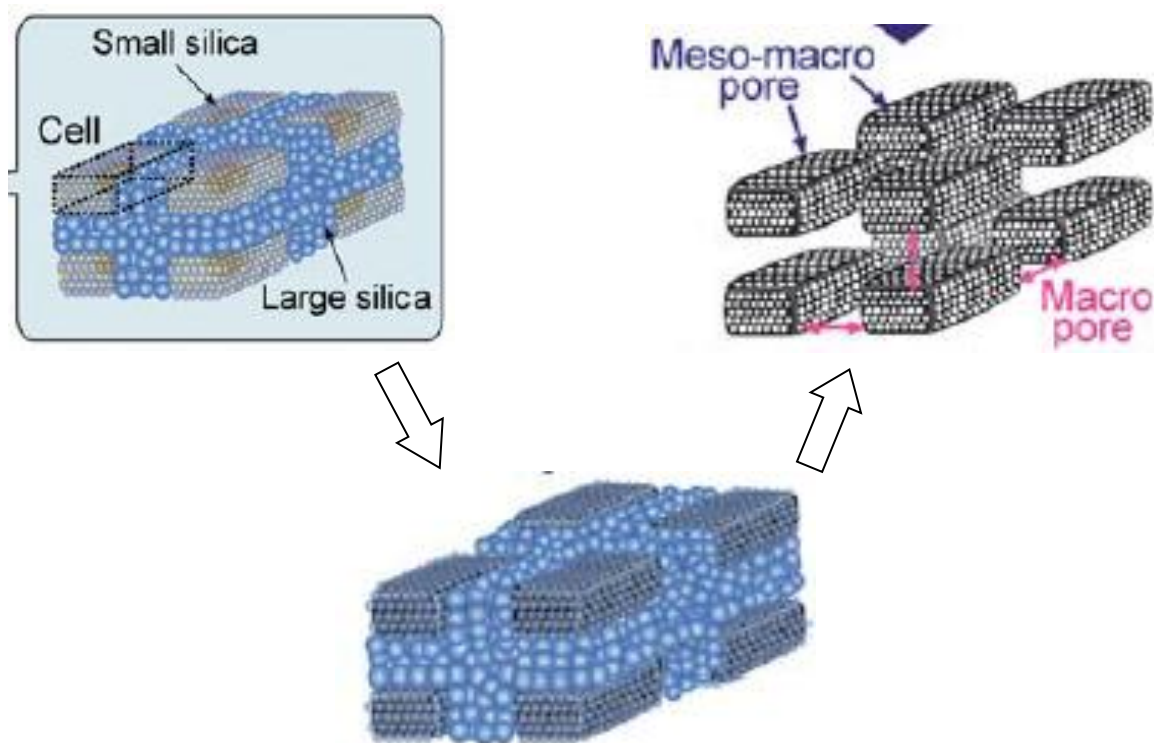


Figure 1.4: Fabrication of hierarchical porous carbon from rice husk (Tabata, et al., 2010).

1.4 Silica/Carbon Composite in Heterogeneous Catalysis

Silica/carbon composite received much attention as heterogeneous catalyst in organic synthesis due to its hybrid organic-inorganic properties. The presence of silica provides durability and thermal stability to this hybrid structure while the carbon matrix could be used for further modification with other functional group (Liu, et al., 2006). For example, the preparation of mesoporous Sn-grafted carbon-silica catalysts for the conversion of sugars into lactic acid and its esters has been demonstrated (de Clippel et al., 2012). This catalyst with dual functionalities as Lewis and weak Brønsted acid sites from Sn and carbon fraction respectively have been proved to catalyze dihydroxyacetone into ethyl lactate efficiently compared to carbon-free Sn-MCM-41.

Functionalization of silica/carbon composite with sulfonic groups has been demonstrated recently (Valle-Vigón, et al., 2012). This mesostructure silica (SBA-15, KIT-6, and mesocellular silica) coated with sulfonic groups-attached carbon have been used in esterification of maleic anhydride, succinic acid and oleic acid with ethanol. This catalyst performed better than commercial acid catalyst such as Amberlyst-15 due to the high density of sulfonic groups and accessibilities of substrate into active site that located inside wide mesopores which allow high mass transfer rate.

Hydrolysis of cellulose into glucose by using sulfonated silica-carbon nanocomposites have been reported (Van de Vyver, et al., 2010). Sulfonic group that attaches on carbon act as strong Brønsted acid sites while silica act as a favourable adsorption site for β -1,4 glucan. As a result, catalyst with higher silica-carbon ratio showed the best catalytic conversion of cellulose. It has been suggested that hydrophilic character of silica facilitate substrate adsorption.

Another example of silica/carbon as catalyst support has been demonstrated (Wan, et al., 2009). In this study, heterogeneous Pd catalysts grafted on ordered mesostructure silica-carbon nanocomposite have been employed in the Heck coupling reaction and in the Ullmann coupling reaction in aqueous media without any phase-transfer catalysts. As a result, ~60% *trans*-stilbene in Heck coupling of chlorobenzene and styrene was produced and of 46% for biphenyl in Ullmann coupling of chlorobenzene was yielded. The factors such as hybrid pore surface constituted by continuous and interpenetrated silica and carbon components, large pore size, uniform dispersion of Pd, and relatively small metal particle size are responsible for high catalytic performance.

The preparation of catalyst from renewable biomaterials such as starch, glucose, maltose, cellulose, and chitosan as carbon precursor is gaining interest recently. Amorphous sulfonated-carbon-silica catalyst for the protection of aldehydes as 1,1-diacetates and for N-, O- and S-acylations has been reported (Gupta & Paul, 2011). It was found that composite derived from starch was the most active catalyst and can be reusable without significant loss of catalytic activity.

1.5 Sugars as Chemical Feedstock

In this era of diminishing petroleum reservoir, researchers around the world have made tremendous efforts to reduce the dependency on crude oil by shifting their focus to use biomass as a chemical feedstock (Huber, et al., 2005). For instance, biodiesel and bioethanol have been used as blending agents for gasoline and diesel. Among biomass products, terpenes have the highest energy content, followed by vegetable oils, lignin, and sugars (Corma et al., 2007). However, due to scarcity of terpenes to meet the requirements, an attention has been shifted towards vegetable oils although there are some issues regarding ethical and limited source.

Figure 1.5 represents the chemical structure of starch and triglycerides, as compared to cellulose. Starch is an α -glycosidic bond of glucose polysaccharide. Therefore, it is very easy to break this bond to produce glucose monomer. The first generation of bioethanol could be obtained facilely from this source.

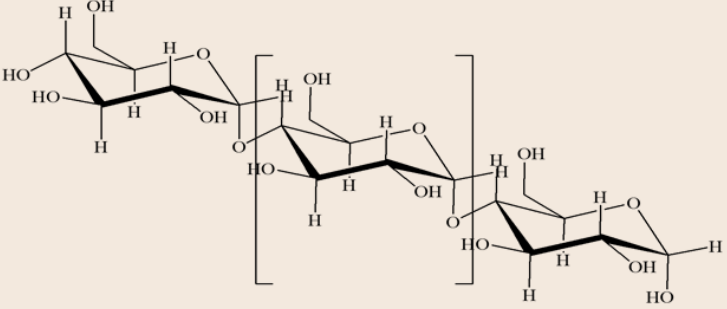
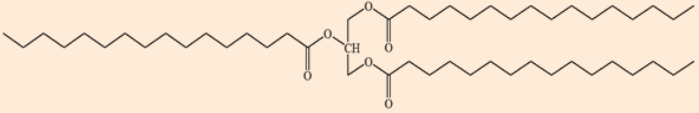
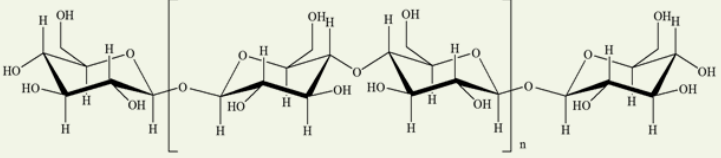
<p>STARCHES</p> <ul style="list-style-type: none"> ○ Corn ○ Beets ○ Sugarcane 	
<p>TRIGLYCERIDES</p> <ul style="list-style-type: none"> ○ Soybean ○ Algae ○ Jatropha 	
<p>CELLULOSE</p> <ul style="list-style-type: none"> ○ Agricultural residues ○ Pulp and paper waste ○ Energy crops 	

Figure 1.5: The biomass feedstock and their chemical structure (Alonso et al., 2010).

Triglycerides are comprised of fatty acid and glycerol, which could be derived from both animal and plant sources. Alas, triglycerides along with starch are not always present in the crops. Instead, lignocellulosic which contributes structural integrity to plants is always present in biomass fraction. It consists of cellulose, hemicelluloses, and lignin, as illustrated in Figure 1.6.

Cellulose is a crystalline glucose polymer connected by β -glycosidic bond. Thus, it is very difficult to break this type of bond, unless a strong acid/harsher condition is used (Lynd, et al., 1991).

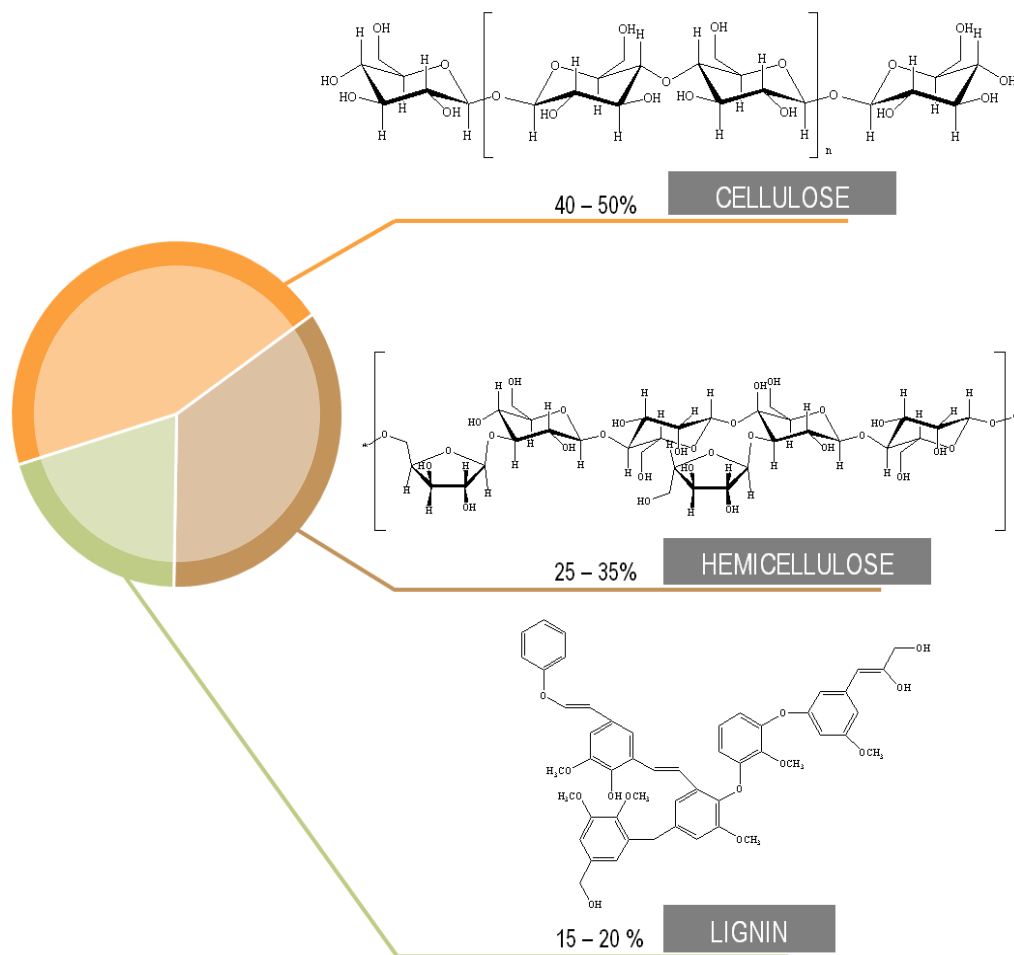


Figure 1.6: Lignocellulosic components in biomass (Alonso, et al., 2010).

However, this condition will favour the formation of HMF, LA, and humins. Hemicellulose is an amorphous polymer that is generally consisting of D-xylose, L-arabinose, D-galactose, D-glucose, and D-mannose, with xylose being the most abundant (Lynd, et al., 1991). Lignin is an amorphous polymer composed of methoxylated phenylpropane structures, such as coniferyl alcohol, sinapyl alcohol, and coumaryl alcohol (Huber, et al., 2006). Lignin which surrounds the hemicellulose and cellulose fractions provide plants with structural rigidity and a hydrophobic vascular system for the transportation of water and solutes (Vanholme, et al., 2008).

Naturally, 170 billion metric tons of biomass is produced per year mainly by photosynthesis while human only consume 3-4% for food and non-food purposes (Röper, 2002). Woody biomass has been identified as largest source of biomass materials despite the fact that essential, yet economical source of sugars could be obtained as compared to corn. Thus, this advancement makes sugars a readily available chemical feedstock for chemicals synthesis. Figure 1.7 demonstrates how biofuels could be derived from different feedstock.

The overabundance of oxygen in sugar's chemical structure could be troublesome especially in selectivity of desired products. In order to lower their oxygen contents, three ways to resolve this problem have been identified (Van Putten, et al., 2013). First method is to eliminate small, highly oxidized carbon molecules, such as CO₂, formaldehyde, and formic acid by means of fermentation to produce ethanol, butanol and CO₂. The second method is hydrogenolysis in which water is formed by removing oxygen from the molecule. The final option is removing water from hexoses. There are some important chemicals that can be derived from dehydration of hexoses in acidic media which have been identified as the basic non-petroleum chemicals; 5-hydroxymethylfurfural (HMF), levulinic acid (LA), and its esters (alkyl levulinate) (Werpy, et al., 2004)

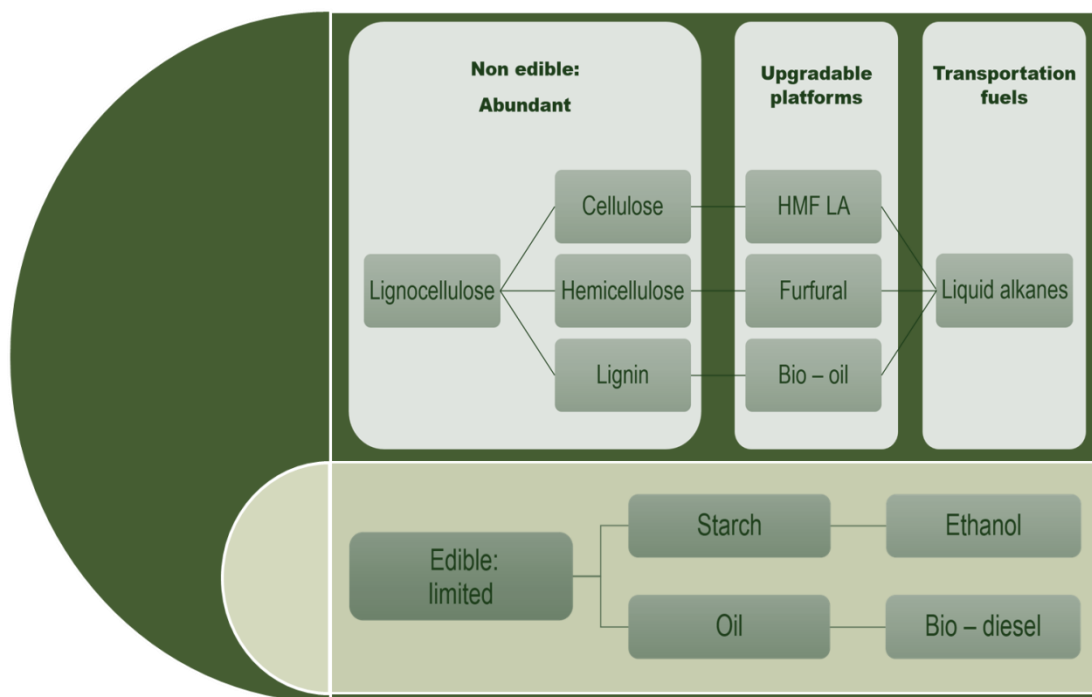


Figure 1.7: Feedstock from biomass and potential as chemical platform for biofuels.

HMF has been identified as a chemical intermediate in biofuel and fine chemicals (Chheda, et al., 2007). HMF stands out among the platform chemicals as it has retained all six carbon atoms. It can be obtained from dehydration of C6 sugars such as glucose and fructose with the presence of acid catalyst, in which the latter is a more reactive substrate (Antal, et al., 1990). The glucose enolyzes in a very low degree and the enolization is a determining step of the HMF formation from glucose. The intricacy to obtain high selectivity and isolated yields render HMF to become costly and thus restrict its potential as a key chemical platform, as illustrated in Figure 1.8.

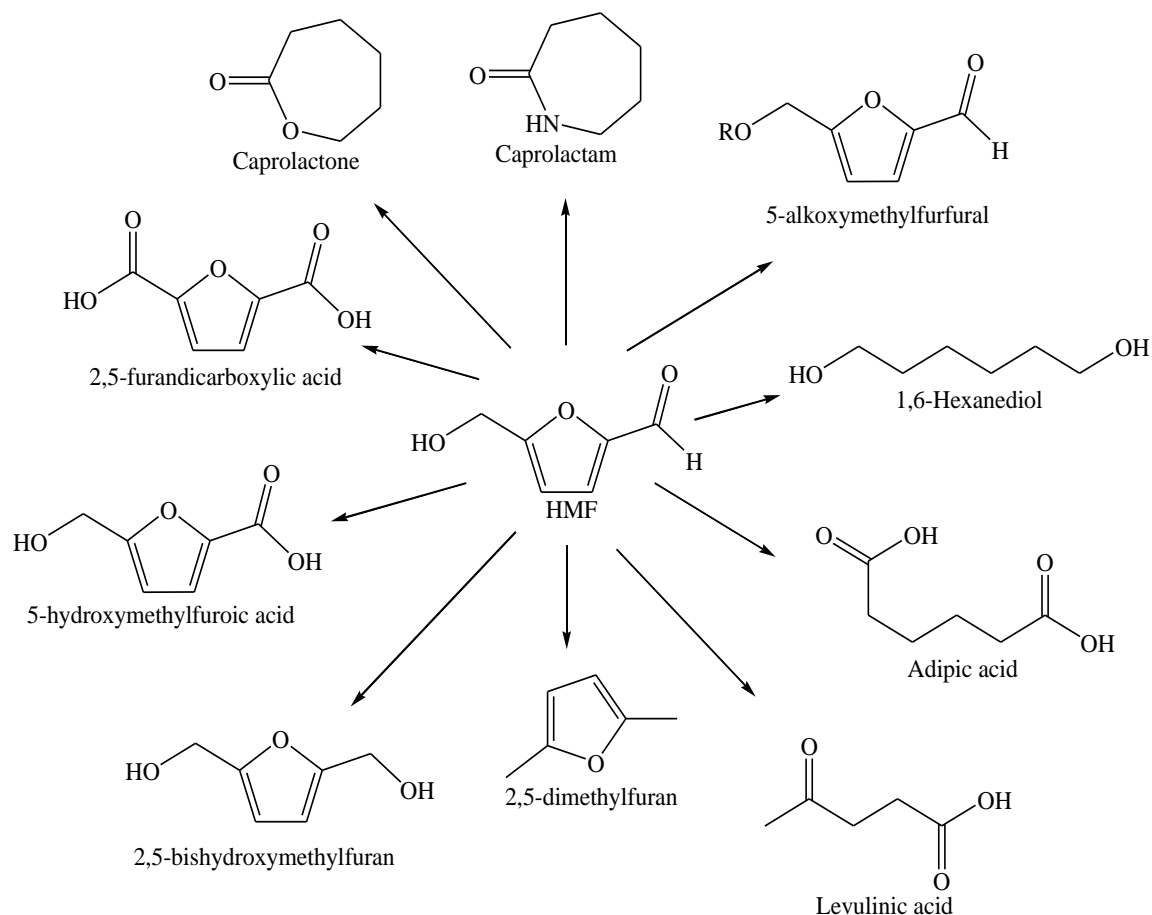


Figure 1.8: Various chemical intermediates from HMF (Van Putten, et al., 2013).

For instance, HMF can be used to produce δ -aminolevulinic acid, an herbicide with a target market of 200-300 lb per year. Remarkably, it also can produce diphenolic acid, a replacement for bisphenol A in polycarbonate production with a target market of 4 billion lb per year. Further rehydration of HMF will produce LA, a highly potential feedstock for herbicide, polymers and petrochemical production. Under alcoholic solvent, sugars can be converted to alkyl levulinates (ALs), commonly used in flavour and fragrance industries and recently has been identified as an additive for gasoline and diesel for transportation fuels (Fagan & Manzer, 2003).

1.6 Mechanism of HMF Formation

In general, the HMF formation from hexoses involves elimination of three molecules of water from the sugar molecule. However, the detail in mechanistic aspect on this conversion is far complicated. Several mechanisms have been proposed in the literature via acyclic and cyclic intermediates.

In acyclic pathways, the formation of a linear 1,2-enediol has been assumed as the rate-limiting step, as depicted in Figure 1.9 (Antal, et al., 1990; Kuster, 1990) which is widely accepted as the intermediate in the aldose-ketose isomerization by the so-called Lobry de Bruyn-Alberda van Ekenstein (LBAE) transformation followed by two consecutive β -dehydrations and a ring closure with a final water elimination to yield HMF (Speck, 1958)

In cyclic pathways, cyclic ketofuranose is a starting form before undergoes the dehydration of the hemiacetal at C2 to form a tertiary carbenium cation. It is followed by two consecutive β -dehydrations in the ring to form HMF. D₂O labeling study verifies this proposed mechanism that irreversible process is taking place after first dehydration as less incorporation of deuterium in HMF structure was observed (Akien, et al., 2012). Thus, it is unlikely for this reaction to proceed via acyclic pathway because it would require the deuterium incorporation during formation of intermediate 3-deoxyglucosone.2,5-anhydro-D-mannose 2,5-anhydro sugar, also refer as chitose, is produced from the first step of D-fructofuranose dehydration. However, since the formation of HMF from chitose was slower than fructose, it was unlikely to become an intermediate (Anet, 1964).

Other researcher was using 2,5-anhydro-L-idose as an intermediate to form HMF (Dekker, 1958). They found that 2,5-anhydro-L-idose reacts 200-300 times faster

than glucose. The formation of C1-aldehyde once undergo dehydration at C2 has been identified as a factor for subsequent dehydration step. ^{13}C NMR study reveals that fructose C-1 forms the carbonyl carbon and fructose C-6 forms the hydroxymethyl carbon of HMF (Zhang & Weitz, 2012). This result confirms plausible mechanism via acyclic and cyclic pathways.

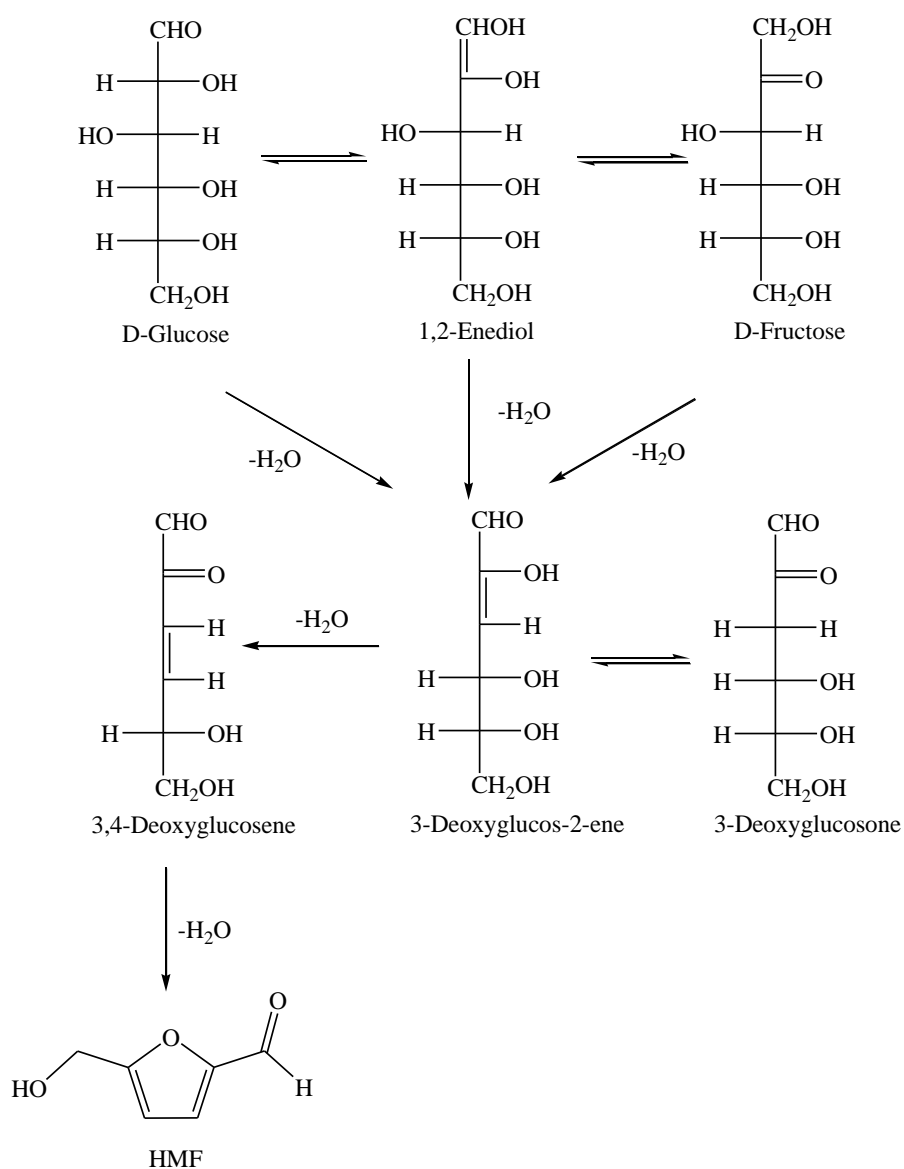


Figure 1.9: Acyclic pathway of HMF formation from hexoses.

The HMF formation could also be achieved by auto-catalysis, especially when using DMSO as a solvent and fructose as a substrate (Amarasekara, et al., 2008). In DMSO, where furanose form is dominant, the O atoms at C1 and C2 are coordinated with DMSO prior to dehydration step, as shown in Figure 1.10.

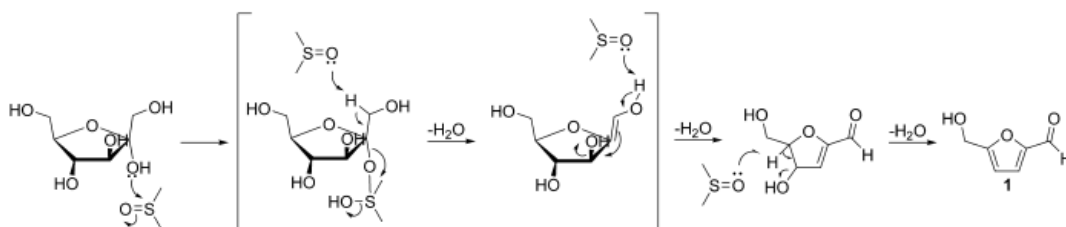


Figure 1.10: Plausible mechanism of fructose dehydration by DMSO as catalyst (Van Putten, et al., 2013).

Besides fructose, glucose could also be converted to HMF and is considered more attractive as the price is cheaper than fructose and could be obtained from lignocellulosic biomass. But, it reacts slower because isomerization of glucose into fructose is necessary before dehydration step to obtain HMF. In the absence of catalyst, glucose conversion in hot compressed water reported the formation of fructose along with HMF. In contrast, no glucose was detected when fructose was treated as a substrate (Watanabe, et al., 2005). This trend even noticeable when operate under higher pressures and temperatures (Aida, et al., 2007). Watanabe et al. (2005) claimed that by using α -TiO₂, this catalyst acts as bifunctional acid-base catalyst. Nevertheless, it enhanced glucose conversion (97% vs 40%) but not HMF yields (22%), as compared to without catalyst. Therefore, it suggests that α -TiO₂ behave as base catalyst that isomerizes glucose into fructose.

Yan et al. (2009) investigated sulphated ZrO_2 and $ZrO_2-Al_2O_3$ as heterogeneous catalyst in this conversion. By using fructose as a substrate, the yield of HMF was similar whether the catalyst was used or not. In comparison, when using glucose as starting material, 48% yield of HMF was obtained with the presence of sulphated $ZrO_2-Al_2O_3$ catalyst and only 4% of HMF without the presence of catalyst. This observation indicates that this catalyst acts as base catalyst that catalyzes glucose isomerization.

It can be concluded that fructose is more reactive to be converted into HMF compare to glucose as the latter requires base catalyst to promote isomerization. Thus, mechanism via cyclic pathway is more likely to take place, as demonstrated in Figure 1.11, since acyclic pathway, so far, does not provide sufficient evident why there is a large gap on catalytic activity and selectivity between glucose and fructose if 1,2-enediol is their common intermediate (Van Putten, et al., 2013).

Besides dehydration, this transformation also involves isomerization, fragmentation, and condensation to yield by-products such as levulinic acid, formic acid, 5-methyl-2-furaldehyde, α -angelica lactone, humins, and many more (Antal, et al., 1990). In fact, aqueous and non-aqueous dehydration processes led to about 37 products.

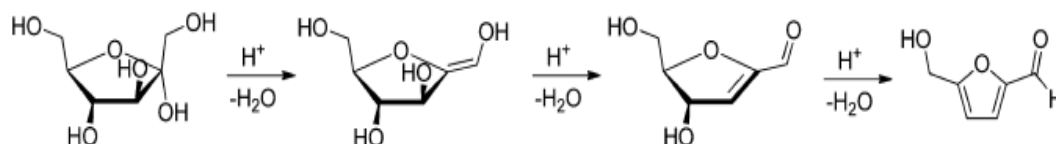


Figure 1.11: Cyclic pathway of HMF formation from fructose (Van Putten, et al., 2013).

1.6.1 HMF Formation from Dehydration of Hexoses by Heterogeneous Catalysts

More efficient and selective formation of HMF can be achieved from dehydration of aldohexose (fructose). Fructose can be obtained from acid hydrolysis of sucrose, inulin and isomerisation of glucose by using homogeneous and heterogeneous acid catalysts. Since heterogeneous acid catalysts is more interesting in term of environmental aspect, the author will be focusing on the use of heterogeneous catalysts.

1.6.1 (a) Aqueous Solvent

Niobic acid and niobium phosphate have been studied as Brønsted heterogeneous catalysts to dehydrate fructose into HMF in aqueous media (Carniti, et al., 2006). Operated at continuous reactor, temperature ranging from 90-110 °C, and pressure from 2-6 bar, niobium phosphate showed better catalytic activity than niobic acid due to effective acidity on the surface. HMF selectivity was higher under flow reactor compare to batch reactor as the fructose concentration increased. Later, they claimed that no side-product from rehydration such as levulinic acid and formic acid were detected. But, the formation of humin was traced.

Carlini et al. (2004) compared vanadyl phosphate (VOP) and substituted VOP with trivalent metals; M^{3+} -VOP ($M = Fe^{3+}, Cr^{3+}, Ga^{3+}, Mn^{3+}, Al^{3+}$) for this reaction. VOP itself gave turn-over frequency (TOF) ~ 200 mmol HMF/g_{cat}h. By substituting Fe^{3+} in the VOP framework, the TOF reached 376. Interestingly, even at higher fructose concentration (40 wt.%), the authors claimed neither insoluble polymeric by-products nor HMF rehydration compounds (levulinic acid and formic acid) were formed.

Qi et al. (2009) tested sulfated zirconia (ZrP) at different calcinations temperatures (500, 600, and 700 °C). They found that in aqueous media, the best calcinations temperature was 600 °C, to give 79.9% fructose conversion and 36% HMF. Asghari & Yoshida (2006) prepared amorphous and crystalline zirconia phosphate catalysts and tested in sub-critical water at 240 °C. As a result, 80% fructose was converted and 61% selectivity of HMF was achieved. They found that no correlation between physicochemical properties and catalytic performances.

Series of layered zirconium- and titanium-hydrogenphosphates in the α and γ structural arrangements, their corresponding α and γ -layered pyrophosphates as well as cubic pyrophosphates were prepared (Benvenuti, et al., 2000). Cubic zirconium pyrophosphate was the most active catalyst (TON = 8.9 mmol HMF/g_{cat}h) followed by γ -titanium phosphate (TON = 6.1 mmol HMF/g_{cat}h). As the reaction time was prolonged to increase fructose conversion, HMF selectivity dropped significantly. The problem was alleviated by applying continuous extraction with methyl isobutyl ketone (MIBK).

An example of mixed-oxides has been demonstrated by Stošić et al. (2012). The preparation of ceria-niobic via coprecipitation methods resulting amphoteric and possess redox centers on their surface. These properties are dependent on the ratio of ceria-to-niobic. The increase of niobic contents increased the catalytic activity as the acid amount of niobic was the highest compare to ceria and ceria-niobic mixed oxides.

Glucose shows to have much lower selectivity for HMF formation because of its more stable ring structure, which hinders its ability to form the acyclicenediol intermediate (Kuster, 1990). This mechanism requires glucose to isomerize to fructose prior to dehydration to HMF.

Zeolite-Y has been tested as heterogeneous catalyst in aqueous glucose solutions (Lourvanij & Rorrer, 1993). Although quantitative glucose conversion was achieved, only <10% of HMF yield was attained while the presence of levulinic acid, formic acid, and coke deposition were also detected.

Chareonlimkun et al. (2010) studied TiO_2 , ZrO_2 and $\text{SO}_4\text{-ZrO}_2$ in hot compressed water at 473-673 K to catalyze HMF formation. TiO_2 (27% yield) and $\text{SO}_4\text{-ZrO}_2$ (22% yield) were identified as the most active catalyst to produce HMF while ZrO_2 was efficient in isomerization. The selection of salt precursor (nitrates and chlorides), sulfur-doping contents, and calcinations temperature (773, 873, and 973 K) of the catalysts were the important factors that influence catalytic activity. Nitrates-based precursor was inferior compared to chlorides-based precursor. The best calcinations temperature was 773 K in which different calcinations temperatures caused different portions of phase to form, as confirmed by XRD. This phase strongly affects acidity-basicity of the catalysts thus affect catalytic performances, as confirmed by NH_3 -TPD and CO_2 -TPD.

Heterogeneous Lewis acid catalyst niobic acid, $\text{Nb}_2\text{O}_5 \cdot n\text{H}_2\text{O}$, has been tested in glucose conversion into HMF in water (Nakajima, et al., 2011). NbO_4 tetrahedra, Lewis acid sites, on niobic acid surface immediately form $\text{NbO}_4\text{-H}_2\text{O}$ adducts in the presence of water. 12.1% of HMF yield was yielded while $\text{Na}^+/\text{Nb}_2\text{O}_5 \cdot n\text{H}_2\text{O}$ without Brønsted acid sites showed similar yield (12.4%). This indicates the formation of HMF under this catalyst system was catalyzed by Lewis acid site alone, as depicted in Figure 1.12.

The formation of unknown products was detected but could not be identified by HPLC and GC-MS. Significant decrease of unknown products was observed when